References

1) Dobrovolskaia MA, McNeil S. Immunological properties of engineered nanomaterials. Nature Nanotechnology 2007; 2: 469-478.
2) Brumfiel G. Nanotechnology: A little knowledge. Nature 2003; 424: 246-248.
3) Dreher KL. Health and environmental impact of nanotechnology: Toxicological assessment of manufactured nanoparticles. Toxicol Sci 2004; 77: 3-5.
4) Giles J. Nanotechnology: What is there to fear from something so small? Nature 2003; 426: 750
5) Hood E. Nanotechnology: Looking as we leap. Environ. Health Perspect 2004; 112: A740-A749
6) Maynard AD, Kuempel E. Airborne nanostructured particles and occupational health. J Nanopart Res 2005; 7: 587-614.
7) Seaton A, Donaldson K. Nanoscience, nanotoxicology, and the need to think small. Lancet 2005; 365: 923-924.
8) Aillon KL, Xie Y, El-Gendy N, Berkland CJ, Forrest ML. Effects of nanomaterial physicochemical properties on in vivo toxicity. Adv Drug Deliv Rev 2009; 61: 457-466.
9) Jia G, Wang HF, Yan L, Wang X, Pei R, Yan T, Zhao Y, Guo X. Cytotoxicity of carbon nanomaterials: single-wall nanotube, multi-wall nanotube, and fullerene. Environ Sci Technol 2005; 39: 1378-1383.
10) Isobe H, Tanaka T, Maeda R, Noiri E, Solin N, Yudasaka M, Iijima S, Nakamura E. Preparation, purification, characterization, and cytotoxicity assessment of water-soluble, transition-metal-free carbon nanotube aggregates. Angew Chem Int Ed 2006; 45: 6676-6680.
11) Johnston HJ, Hutchinson GR, Christensen FM, Peters S, Hankin S, Srone V. Identification of the mechanisms that drive the toxicity of TiO2 particles: the contribution of phycochemical characteristics. Part Fibre Toxicol 2009; 6: 1-33.
12) Braydich-Stolle LK, Schaeubin NM, Murdock RC, Jiang J, Biswas P, Schlager JJ, Hussain SM. Crystal structure mediates mode of cell death in TiO2 nanotoxicity. J Nanopart Res 2009; 11: 1361-1374.
13) Mosmann T. Rapid colorimetric assay for cellular growth and survival: Application to proliferation and cytotoxicity assays. J Immunol Methods 1983; 65: 55-63.
14) Liu Y, Peterson DA, Kimura H, Schubert D. Mechanism of cellular 3-(4,5-Dimethyl-2-thiazolyl)-2,5-diphenyl-2H tetrazolium bromide (MTT) reduction. J Neurochem 1997; 69, 581-593.
15) Pereira C, Oliveira CR. Oxidative glutamate toxicity involves mitochondrial dysfunction and perturbation of intracellular Ca2+ homeostasis. Neurosci Res 2000; 37: 227-236.
16) Jones KH, Senft JA. An Improved Method to Determine Cell Viability by Simultaneous Staining with Fluorescein Diacetate-Propidium Iodide, J Histochem Cytochem 1985; 33, 77-79.
17) Taylor IW, Milthorpe BK. An Evaluation of DNA Fluochromes, Staining Techniques, and Analysis for Flow Cytometry. I. Unperturebed Cellpopulations. J Histochem Cytochem 1980; 28: 1224-1232.
18) Vuist WMJ, Buitenen FV, De Rie MA, Hekman A, Ruemke P, Melief CJM. Potentiation by Interleukin 2 of Burkitt's Lymphoma Therapy with Anti-Pan B (Anti-CD19) Monoclonal Antibodies in a Mouse Xenotransplantation Model. Cancer Res 1989; 49: 3783-3788.
19) El-Naggar AK, Batsakis JG, Teague K, Garnsey L, Barlogie B. Single- and Double-stranded RNA Measurements by Flow Cytometry in Solid Neoplasms. Cytometry 1991; 12: 330-335.
20) Souchier C, Ffrench M, Benchaib M, Catallo R, Bryon PA. Methods for Cell Proliferation Analysis by Fluorescent Image Cytometry. Cytometry 1995; 20: 203-209.
21) Korzeniewski C, Callewaert DM. An enzyme-release assay for natural cytotoxicity. J Immunol Meth 1983; 64: 313-20.
22) Decker T, Lohmann-Matthes ML. (1988) A quick and simple method for the quantitation of lactate dehydrogenase release in measurements of cellular cytotoxicity and tumor necrosis factor (TNF) activity. J Immunol Meth 1988; 115: 61-9.
23) Hanagata N, Zhuang F, Connolly S, Li J, Ogawa N, Xu M. Molecular response to CuO nanoparticle toxicity in human lung epithelial cells. ACS Nano 5:9326-9338 (2011)
24) Midander K, Cronholm P, Karlsson HL, Elihn K, Moeller L, Leygraf C, Wallinder IO. Surface characteristics, copper release, and toxicity of nano- and micrometer-sized copper and copper(II) oxide particles: A cross-disciplinary study. Small 2009; 5: 389-399.
25) Xu L, Takemura T, Xu M, Hanagata N. Toxicity of silver nanoparticles as assessed by global gene expression analysis. Mater Expr 2011; 1: 74-79.
26) Karlsson HL, Cronholm P, Gustafsson J, Moeller L. Copper oxide nanoparticles are highly toxic: A comparison between metal oxide nanoparticles and carbon nanotubes. Chem Res Toxicol 2008; 21: 1726-1732.
27) Deng X, Luan Q, Chen W, Wang Y, Wu M, Zhang H, Jiao Z. Nanosized zinc oxide particles induce neural stem cell apoptosis. Nanotechnology 2009; 20: 115101(7pp)
28) Lin W, Xu Y, Huang C-C, Ma Y, Shannon KB, Chen D-R, Huang Y-W. Toxicity of nano- and micro-sized ZnO particles in human lung

epithelial cells. J Nanopart Res 2009; 11: 25-39.
29) Sasidharan A, Chandran P, Menon D, Raman S, Nair S, Koyakutty M. Rapid dissolution of ZnO nanocrystals in acidic cancer microenvironment leading to preferential apoptosis. Nanoscale 3:3657-3669 (2011)
30) Risom L, Moller P, Loft S. Oxidative stress-induced DNA damage by particular air pollution. Mutat Res 2005; 592: 119-137.
31) Ai H, Bu Y, Han K. Glycine-Zn+/Zn2+ and their hydrates: on the number of water molecules necessary to stabilize the zwitterionic glycine-Zn+/Zn2+ over the nonzwitterionic ones. J Chem Phys 2003; 118: 10973-10985.
32) Xia T, Kovochich M, Liong M, Madler L, Gilbert B, Shi H, Yeh JI, Zink JI, Nel AE. Comparison of the mechanism of toxicity of zinc oxide and cerium oxide nanoparticles based on dissolution and oxidative stress properties. ACS Nano 2008; 2: 2121-2134.
33) Li N, Sioutas C, Cho A, Schmitz D, Misra C, Sempf J, Wang M, Oberley T, Froines J, Nel A. Ultrafine particle pollutants induce oxidative stress and mitochondrial damage. Environ Health Perspect 2003; 111: 455-460.
34) AshaRani PV, Low Kah MG, Hande MP, Valiyaveettil S. Cytotoxicity and genotoxicity of silver nanoparticles in human cells. ACS Nano 2009b; 3: 279-290.
35) Shvedova AA, Kagan VE. The role of nanotoxicology in realizing the 'helping without harm' paradigm of nanomedicine: lessons from studies of pulmonary effects of single-walled carbon nanotubes. J Internal Med 2010; 267: 106-118.
36) Johnston HJ, Hutchison GR, Christensen FM, Peters S, Hankin S, Aschberger K, Stone V. A critical review of the biological mechanisms underlaying the in vivo and in vitro toxicity of carbon nanotubes: The contribution of physic-chemical characteristics. Nanotoxicology 2010; 4: 207-246.
37) Hu XK, Cook S, Wang P, Hwang HM, Liu X, Williams QL. In vitro evaluation of cytotoxicity of engineered carbon nanotubes in selected human cell lines. Sci Total Environ 2010; 408: 1812-1817.
38) Pulskamp K, Diabate S, Krug HF. Carbon nanotubes show no sign of acute toxicity but induce intracellular reactive oxygen species in dependence on contaminats. Toxicol Lett. 2007, 168:58-74.
39) Vittorio O, Raffa V, Cuschieri A. Influence of purity and surface oxidation on cytotoxicity of multiwalled carbon nanotubes with human neuroblastma cells. Nanomedicine: NBM 2009; 5: 424-431.
40) Ostrovsky S, Kazimirsky G, Gedanken A, Brodie C. Selective cytotoxic effect of ZnO nanoparticles on glioma cells. Nano Res 2009; 2:882-890.
41) Hanley C, Thurber A, Hanna C, Punnoose A, Zhang JH, Winngett DG. The influences of cell type and ZnO nanoparticles size on immune cell cytotoxicity and cytokine induction. Nanoscale Res Lett 2009; 4: 1409-1420.
42) Yang H, Wu QY, Tang M, Kong L, Lu ZH. Cell membrane injury induced by silica nanoparticles in mouse macrophage. J Biomed Nanotech 2009a; 5: 528-535.
43) Huang CC, Aronstam RS, Chen DR, Huang YW. Oxidative stress, calcium homeostasis, and altered gene expression in human lung epithelial cells exposed to ZnO nanoparticles. Toxicol In Vitro 2010; 24: 45-55.
44) AshaRani PV, Hande MP, Valiyaveettil S. Anti-proliferative activity of silver nanoparticles. BMC Cell Biol. 2009; 10: 65.
45) Moutin MJ, Abramson JJ, Salama G, Dupont Y. Rapid Ag+-induced release of Ca2+ from sarcoplasmic reticulum vesicles of skeletal muscle: a rapid filtration study. Biochem Biophys Acta 1989; 984: 289-292.
46) Yang H, Liu C, Yang DF, Zhang HS, Xi ZG. Comparative study of cytotoxicity, oxidative stress and genotoxicity induced by four typical nanomaterials: the role of particle size, shape and composition. J Appl Toxicol 2009b; 29: 69-78.
47) Sharma V, Shukla RK, Saxena N, Parmar D, Das M, Dhawan A. DNA damaging potential of zinc oxide nanopaticles in human epidermal cells. Toxicol Lett 2009; 185: 211-218.
48) Gerloff K, Albrecht C, Boots AW, Forster I, Schins RPF. Cytotoxicity and oxidative DNA damage by nanoparticles in human intestinal CaCo-2 cells. Nanotoxicology 2009; 3: 255-264.
49) Fahmy B, Cormier SA. Copper oxide nanoparticles induce oxidative stress and cytotoxicity in airway epithelial cells. Toxicol In Vitro 2009; 23: 1365-1371.
50) Alarifi S., Ali D., Alkahtani., Verma A., Ahamed M., Ahmed M., Alhadlaq HA. Induction of oxidative stress, DNA damage, and apoptosis in a malignant human skin melanoma cell line after exposure to zinc oxide nanoparticles. Int. J. Nanomed. 8: 983-993 (2013)
51) Hanagata N, Xu M,Takemura T, Zhuang F. Cellular responses to ZnO nanoparticles inferred from global gene expression analysis. Nano Biomed 2010; 2: 153-169.
52) Wang F, Gao F, Lan MB, Yuan HH, Huang YP, Liu JW. Oxidative stress contributes to silica nanoparticle-induced cytotoxicity in human embryonic kidney cells. Toxicol In Vitro2009; 23: 808-815.

53) Andrews GK. Regulation of metallothionein gene expression by oxidative stress and metal ions. Biochem Pharmacol 2000; 59: 95-104.
54) Huang Y-C T, Li Z, Carter JD, Soukup JM, Schwartz DA, Yang IV. Fine ambient particles induce oxidative stress and metal binding genes in human alveolar macrophages. Am J Respir Cell Mol Biol 2009; 41: 544-552.
55) Min KS, Morishita F, Tetsuchikawahara N, and Onosaka S. Induction of hepatic and renal metallothionein synthesis by ferric nitrilotriacetate in mice: the role of MT as an antioxidant. Toxicol Appl Pharmacol 2005; 204: 9–17.
56) Kumai MVR, Hiramatsu M, Ebadi M. Free radical scavenging actions of metallothionein isoforms I and II. Free Rad Res 1998;29:93-101.
57) Sato M, Kondoh M. Recent studies on metallothionein: protection agaist toxicity of heavy metals and oxygen free radicals. The Tohoku J Exp Med 2002; 196: 9-22.
58) Bauman JW, Madhu C, McKim Jr JM, Liu Y, Klaassen CD. Induction of hepatic metallothionein by paraquat. Toxicol Appl Pharmacol 1992; 117: 233-241.
59) Dalton T, Palmiter RD, Andrews GK. Transcriptional induction of the mouse metallothionein-I gene in hydrogen peroxide-treated Hepa cells involves a composite major late transcription factor/antioxidant response element and metal response promoter elements. Nucleic Acid Res 1994; 22: 5016-5023.
60) Thornalley PJ, Vasak M. Possible role for metallothionein in protection against radiation-induced oxidative stress. Kinetics and mechanism of its reaction with superoxide and hydroxyl radicals. Biochim Biophys Acta 1985; 827: 36-44.
61) Vliagoftis H, Schwingshackl A, Milne CD, Duszyk M, Hollenberg MD, Wallace JL, Befus AD, Moqbel R. Proteinase-activated receptor-2-mediated matrix metalloproteinase-9 release from airway epithelial cells. J Allergy Clinic Immunol 2000; 106: 537-545.
62) Ye YY, Liu JW, Xu JH, Sun LJ, Chen MC, Lan MB. Nano-SiO2 induces apoptosis via activation of p53 and Bax mediated by oxidative stress in human hepatic cell line. Toxicol In Vitro 2010; 24: 751-758.
63) Jayasurya A, Bay BH, Yap WM, Tan NG. Correlation of metallothionein expression with apoptosis in nasapharyngeal carcinoma. Brit J Cancer 2000; 82: 1198–1203.
64) Donaldson K, Tran CL. Inflammation caused by particles and fibers. Inhal Toxicol 2002; 14: 5-27.
65) Donaldeson K, Tran L, Jimenez LA, Duffin R, Newby DE, Mills N, MacNee W, Stone V. Combursion-derived nanoparticles: A review of their toxicology following inhalation exposure. Part Fibre Toxicol 2005; 2: 10.
66) Wu WS, Tsai RK, Chang CH, Wang S, Wu JR, Chang YX. Reactive oxygen species mediated sustained activation of protein kinase C and ERK for migration of human hepatoma cell HepG2. Mol Cancer Res 2006; 4:747-58.
67) Valko M, Rhodes CJ, Moncol J, Izakovic M, Mazur M. Free radicals, metals and antioxidants in oxidative stress induced cancer. Chem Biol Interact 2006; 160:1-40.
68) Hussain SM, Hess KL, Gearhart JM, Geiss KT, Schlager JJ. In vitro toxicity of nanoparticles in BRL 3A rat liver cells. Toxicol In Vitro 2005; 19:975-83.
69) Carlson C, Hussain SM, Schrand AM, Braydich-Stolle LK, Hess KL, Jones RL, Schlager JJ. Unique cellular interaction of silver nanoparticles: size-dependent generation of reactive oxygen species. J Phys Chem 2008; 112:13608-19.
70) Hsin, YH, Chen CF, Huang S, Shih TS, Lai PS, Chueh PJ. The apoptosis effect of nanosilver is mediated by a ROS- and JNK-dependent mechanism involving the mitochondrial pathway in NIH3T3 cells. Toxicol Lett 2008; 197:130-9.
71) Xia T, Kovochich M, Brant J, Hotze M, Sempf J, Oberley T, Sioutas C, Yeh JI, Wiesner MR, Nel AE. Comparison of the abilities of ambient and manufactured nanoparticles ti induce cellular toxicity according to an oxidative stress paradigm. Nano Lett 2006; 6:1794-807.
72) Foldbjerg R, Dang DA, Autrup H. Cytotoxicity and genotoxicity of silver nanoparticles in the human lung cancer cell line, A549. Arch Toxicol. 2011, 85:743-50.
73) Beru Be K, Balharry D, Sexton K, Koshy L, Jones T. Combustion-derived nanoparticles: Mechanisms of pulmonary toxicity. Clin Exp Pharmacol Physiol 2007; 34: 1044-1050.
74) Schins RP. Mechanisms of genotoxicity of particles and fibers. Inhal Toxicol 2002; 14: 57-78.
75) Schins RP, Knappen AM, Cakmak GD, Shi T, Weishaupt C, Borm PJ. Oxidant-induced DNA damage by quartz in alveolar epithelial cells. Mutat Res 2002; 517: 77-86.

(Received: May 31, 2013/
Accepted: June 23, 2013)

Corresponding author:
Prof. Nobutaka Hanagata
Nanotechnology Innovation Station,
National Institute for Materials Science
1-2-1 Sengen, Tsukuba, Ibaraki 305-0047, Japan
Tel: +81-29-860-4774
Fax: +81-29-859-2475
E-mail: HANAGATA.Nobutaka@nims.go.jp

OPEN ACCESS
IOP PUBLISHING
SCIENCE AND TECHNOLOGY OF ADVANCED MATERIALS
Sci. Technol. Adv. Mater. 14 (2013) 055009 (10pp)
doi:10.1088/1468-6996/14/5/055009

Preparation and characterization of multifunctional magnetic mesoporous calcium silicate materials

Jianhua Zhang[1], Yufang Zhu[2], Jie Li[3], Min Zhu[2], Cuilian Tao[1] and Nobutaka Hanagata[3]

[1] School of Medical Instrument and Food Engineering, University of Shanghai for Science and Technology, 516 Jungong Road, Shanghai 200093, People's Republic of China
[2] School of Materials Science and Engineering, University of Shanghai for Science and Technology, 516 Jungong Road, Shanghai 200093, People's Republic of China
[3] Interdisciplinary Laboratory for Nanoscale Science and Technology, National Institute for Materials Science, 1-2-1 Sengen, Tsukuba, Ibaraki 305-0047, Japan

E-mail: zjf2412@163.com

Received 14 July 2013
Accepted for publication 26 September 2013
Published 22 October 2013
Online at stacks.iop.org/STAM/14/055009

Abstract

We have prepared multifunctional magnetic mesoporous Fe–$CaSiO_3$ materials using triblock copolymer (P123) as a structure-directing agent. The effects of Fe substitution on the mesoporous structure, *in vitro* bioactivity, magnetic heating ability and drug delivery property of mesoporous $CaSiO_3$ materials were investigated. Mesoporous Fe–$CaSiO_3$ materials had similar mesoporous channels (5–6 nm) with different Fe substitution. When 5 and 10% Fe were substituted for Ca in mesoporous $CaSiO_3$ materials, mesoporous Fe–$CaSiO_3$ materials still showed good apatite-formation ability and had no cytotoxic effect on osteoblast-like MC3T3-E1 cells evaluated by the elution cell culture assay. On the other hand, mesoporous Fe–$CaSiO_3$ materials could generate heat to raise the temperature of the surrounding environment in an alternating magnetic field due to their superparamagnetic property. When we use gentamicin (GS) as a model drug, mesoporous Fe–$CaSiO_3$ materials release GS in a sustained manner. Therefore, magnetic mesoporous Fe–$CaSiO_3$ materials would be a promising multifunctional platform with bone regeneration, local drug delivery and magnetic hyperthermia.

Keywords: mesoporous calcium silicate, magnetic hyperthermia, drug delivery, bone regeneration

1. Introduction

Calcium silicate ($CaSiO_3$) materials, a classic example of Ca–Si-based bioceramics, have been proposed as potential bioactive materials for bone tissue regeneration due to their excellent bioactivity and degradability [1–4]. Studies demonstrated that biomaterials with high specific surface area and pore volume could accelerate the kinetic process of apatite formation and therefore, enhance the bone-forming bioactivity [5, 6]. In recent years, many efforts have been made to develop mesoporous $CaSiO_3$ materials for bone regeneration [7–12], because mesoporous materials have unique structural characteristics including high specific surface area, large pore volume and controllable porosity at mesoscale [13]. Li *et al* [7] synthesized mesoporous $CaSiO_3$ materials using mesoporous silica SBA-15 as the template and silicon source, which exhibited a significantly enhanced bone-forming ability compared to the conventional

amorphous $CaSiO_3$ materials. Chang and co-workers [8, 9] prepared mesoporous $CaSiO_3$ materials using the surfactant templating method to study its potential application in filling the apical root canals of teeth. In addition, Wei *et al* [10] and Zhu *et al* [11] designed mesoporous $CaSiO_3$/polymer composites for potential use in hard tissue repair. On the other hand, mesoporous materials have been considered as promising carriers for drug delivery [13, 14], and mesoporous $CaSiO_3$ nanoparticles could also exhibit sustained drug delivery ability [12]. Therefore, mesoporous $CaSiO_3$ materials with local drug delivery would be beneficial for bone regeneration.

Generally, both texture and composition of bioceramics control their physicochemical and biological properties [15–17]. Studies demonstrated that the incorporation of zinc (Zn), strontium (Sr), titanium (Ti) or magnesium (Mg) in $CaSiO_3$ ceramics improved their physicochemical and biological properties [18–24]. For example, Ramaswamy *et al* [19] incorporated Zn into Ca–Si system to form $Ca_2ZnSi_2O_7$ ceramics, and found that $Ca_2ZnSi_2O_7$ ceramics supported osteoblast-like cells attachment with a well-organized cytoskeleton structure and significantly increased cellular proliferation and differentiation compared to $CaSiO_3$ ceramics. Lu *et al* [23] synthesized a mesoporous magnesium–$CaSiO_3$, which could support cell attachment and promote the proliferation and differentiation of MC3T3-E1 cells. We recently substituted Sr into mesoporous $CaSiO_3$ materials, and found that the mesoporous Sr–$CaSiO_3$ materials kept mesoporous structure and enhanced the proliferation and alkaline phosphatase activity of MC3T3-E1 cells compared to the mesoporous $CaSiO_3$ materials [24].

Iron (Fe) plays a vital role in the functioning of body with Fe pool in humans being found in the red blood cells, with a lesser extent in the tissues and a small amount circulating in the plasma [25]. Studies demonstrated that the Fe-containing bioceramics could stimulate their cell response ability [26–29]. For example, Wu *et al* [26] fabricated a CaP ceramic–magnetite nanoparticles (CaP–MNP) composite, and the *in vitro* results indicated that the CaP–MNP composite was able to significantly promote Ros17/2.8 and MG63 cells' proliferation and differentiation compared to ordinary CaP ceramics. Panseri *et al* developed magnetic hydroxyapatite scaffolds to enhance tissue regeneration. The hydroxyapatite/magnetite 90/10 scaffolds were shown to enhance cell proliferation at the early stage, and a good level of histocompatibility was observed in a critical size lesion of the rabbit condyle *in vivo* [27]. On the other hand, studies demonstrated that magnetic bioceramics could generate heat under alternating magnetic field and be used for hyperthermia therapy in bone defects caused by bone tumors [30–33], because cancer cells generally perish around 43 °C due to hemorrhage, stasis and vascular occlusion, whereas normal cells are not damaged until higher temperature [33, 34].

Therefore, we hypothesized that mesoporous Fe-doped $CaSiO_3$ (Fe–$CaSiO_3$) materials could induce an improved bone-forming bioactivity and stimulate bone cell growth due to the mesoporous structure and the Fe incorporation. Furthermore, mesoporous Fe–$CaSiO_3$ materials could effectively load drugs or growth factors as a potential local drug delivery system, and could be magnetic seeds for magnetic hyperthermia treatment. It can be believed that mesoporous Fe–$CaSiO_3$ materials would be a promising multifunctional platform with bone regeneration, local drug delivery and magnetic hyperthermia for the treatment of bone defects caused by bone tumors after surgery. Recently, magnetic mesoporous iron oxide and silica particles were developed for drug delivery and hyperthermia therapy, but they were not bioactive for bone regeneration [32, 35–37]. We prepared magnetic mesoporous bioactive glass scaffolds, which showed the potential for bone regeneration with bioactivity, sustained drug delivery and magnetic hyperthermia properties [38, 39]. However, the preparation procedure was multistep and rather complex. To the best of our knowledge, there are no previous reports describing the preparation of magnetic mesoporous Fe–$CaSiO_3$ materials and further investigating their multifunctionality for bone regeneration.

In this study, we have successfully prepared magnetic mesoporous Fe–$CaSiO_3$ materials using triblock copolymer (P123) as a structure-directing agent. The effects of the Fe substitution on the mesoporous structure, magnetic heating ability and *in vitro* bioactivity of mesoporous $CaSiO_3$ materials have been investigated. Gentamicin, an antibiotic for treating osteomyelitis, was used as a model drug and introduced into mesoporous Fe–$CaSiO_3$ materials to evaluate the drug delivery property.

2. Experimental methods

2.1. Preparation and characterization of mesoporous Fe–$CaSiO_3$ materials

Mesoporous Fe—$CaSiO_3$ materials were prepared according to the previously reported method with some modifications [8]. The chemical compositions and the sample names are listed in table 1. In a typical synthesis for mesoporous 5%Fe–$CaSiO_3$ materials, 3.0 g of P123 (Mw = 5800, Aldrich) was dissolved in 130 ml of H_2O and 20.5 ml of HCl (⩾37%, Sigma-Aldrich) while stirring at 38 °C in oil bath until the solution became clear. After the addition and dissolution of 9.15 g of $Ca(NO_3)_2 \cdot 4H_2O$ (Aldrich) and 0.824 g of $Fe(NO_3)_3 \cdot 9H_2O$ (Aldrich) in P123 solution, 8.5 g of tetraethyl orthosilicate (TEOS, 98%, Aldrich) was then added into the solution. The mixture was stirred at 38 °C for 24 h, and the resulting precipitate was dried at 100 °C for 24 h in air without any filtering and washing. The as-synthesized materials were calcined from room temperature to 600 °C with a heating rate of 1 °C min^{-1}, and maintained at 600 °C for 6 h to remove the templates. Finally, the calcined materials were treated in 10% H_2 per 90% Ar at 400 °C for 3 h to obtain magnetic mesoporous Fe–$CaSiO_3$ materials.

The wide angle x-ray diffraction patterns were obtained on a Stoe Stadi P powder diffractometer equipped with a curved germanium (111) monochromator and linear

Table 1. Chemical composition and the reactants of mesoporous Fe–$CaSiO_3$ materials.

Sample names	Fe:Ca:Si (molar ratio)	P123 (g)	$Ca(NO_3)_2 \cdot 4H_2O$ (g)	$Fe(NO_3)_3 \cdot 9H_2O$ (g)	TEOS (g)	H_2O (ml)	HCl (ml)
0Fe–$CaSiO_3$	0:100:100	3	9.64	0	8.5	130	20.5
5Fe–$CaSiO_3$	5:95:100	3	9.15	0.82	8.5	130	20.5
10Fe–$CaSiO_3$	10:90:100	3	8.67	1.65	8.5	130	20.5

position-sensitive detector using Cu Kα1 radiation (1.5405 Å) in transmission geometry. Scanning electron microscopy (SEM) was carried out with an FEI Quanta 450 field emission scanning electron microscope. Transmission electron microscopy (TEM) was performed with a JEM-2010 electron microscope operated at an acceleration voltage of 200 kV. N_2 adsorption–desorption isotherms were obtained on a Quadrasorb SI automated surface area and pore size analyzer at −196 °C under continuous adsorption condition. Brunauer–Emmett–Teller (BET) and Barrett–Joyner–Halenda (BJH) methods were used to determine the surface area, the pore size distribution and the pore volume. Magnetic measurement was performed using a vibrating sample magnetometer.

2.2. Ion dissolution and apatite formation of mesoporous Fe–CaSiO_3 materials in simulated body fluids (SBF)

To investigate the ion dissolution from mesoporous Fe–$CaSiO_3$ materials, the SBF were prepared according to Kokubo's method [40]. Mesoporous Fe–$CaSiO_3$ materials were soaked in the SBF solutions at 37 °C for 1, 3, 5 and 7 days, and the ratio of mesoporous Sr–$CaSiO_3$ mass to the SBF volume was 2 mg ml^{-1}. The concentrations of the Ca, Si and Fe ions in the SBF solutions were determined by inductively coupled plasma optical emission spectrometer (ICP-OES, Shimadzu ICPS-8100). The pH values of the SBF solutions were measured after soaking mesoporous Fe–$CaSiO_3$ materials at predetermined time intervals.

The apatite formation ability of mesoporous Fe–$CaSiO_3$ materials was also carried out in the SBF solution. Typically, 0.1 g of mesoporous Fe–$CaSiO_3$ material was compacted into a pellet of 6 mm diameter by uniaxial compression at 3 MPa. Mesoporous Fe–$CaSiO_3$ pellets were soaked in the SBF solution in a polyethylene bottle at 37 °C for different periods ($M_{Fe-CaSiO3}/V_{SBF} = 2$ mg ml^{-1}). After soaking, mesoporous Fe–$CaSiO_3$ pellets were collected from the SBF solution, rinsed with ethanol and dried. SEM observations and energy-dispersive x-ray spectroscopy (EDS) measurements were used to study the apatite formation on the surfaces of mesoporous Fe–$CaSiO_3$ pellets.

2.3. Cytotoxicity evaluation of mesoporous Fe–CaSiO_3 materials

To investigate the cytotoxicity of mesoporous Fe–$CaSiO_3$ materials, Osteoblast-like MC3T3-E1 cells and WST-8 assay were used in this study. Prior to the cytotoxicity evaluation, the extracts of mesoporous Fe–$CaSiO_3$ materials were prepared in culture medium according to International Standard Organization (ISO/EN) 10993-5,[4] by adding mesoporous Fe–$CaSiO_3$ materials to serum-free α-MEM medium (without L-glutamine or ascorbic acid) at a final concentration of 50 mg ml^{-1}. After incubating at 37 °C for 24 h, the mixtures were centrifuged and the supernatants collected. Serial dilutions of extracts (25, 12.5 and 6.25 mg ml^{-1}) were prepared using serum-free α-MEM medium. The diluted extracts were filter sterilized and used for subsequent MC3T3-E1 cell culture experiments.

To evaluate the cytotoxicity of mesoporous Fe–$CaSiO_3$ materials, MC3T3-E1 cells were seeded at a density of 5×10^3 cells cm^{-2} into a 96-well plate with regular α-MEM medium and incubated for 24 h, after which the medium was removed and replaced by 50 μl of α-MEM medium supplemented with 20% FBS and 50 μl of diluted extracts. For a blank control, 100 μl of α-MEM medium supplemented with 10% FBS but without the addition of diluted extracts was used. The cells were incubated at 37 °C in a humidified 5% CO_2 atmosphere for 7 days. Subsequently, WST-8 (cell counting kit-8, CCK-8) assay was performed by adding 10 μl of CCK-8 solution to each well and incubated for 3 h at 37 °C to form WST-8 formazan. The absorbance of the WST-8 formazan was read at 450 nm on a microplate reader (MTP-880, Corona). The results were expressed as the absorbance reading from each well less the optical density value of a blank.

2.4. Magnetic heating property of magnetic mesoporous Fe–CaSiO_3 materials

For the magnetic heating experiment, a high-frequency generator (power 5 kW) was used. The used inductor was a water-cooled copper coil with 11 turns on a length of 105 mm and a diameter of 42.5 mm. For measurement, an open-top vessel with a dispersion of magnetic mesoporous Fe–$CaSiO_3$ materials (100 mg ml^{-1}) was placed in the inductor. While applying the alternating magnetic field, the temperature was monitored using a pyrometer that was placed above the inductor and focused on the dispersion surface. To obtain the heating curve of the magnetic mesoporous Fe–$CaSiO_3$ materials, a reference measurement of the pure solvent (equivalent volume) was subtracted from the data.

2.5. Loading and in vitro *release of gentamicin*

1.0 g of mesoporous Fe–$CaSiO_3$ materials was immersed in 40 ml of gentamicin solution (10 mg ml^{-1}). After 24 h, the drug-loaded mesoporous Fe–$CaSiO_3$ materials were

[4] ISO/EN 10993-5. Biological evaluation of medical devices—part 5 tests for cytotoxicity, in vitro methods: 8.2 tests on extracts.

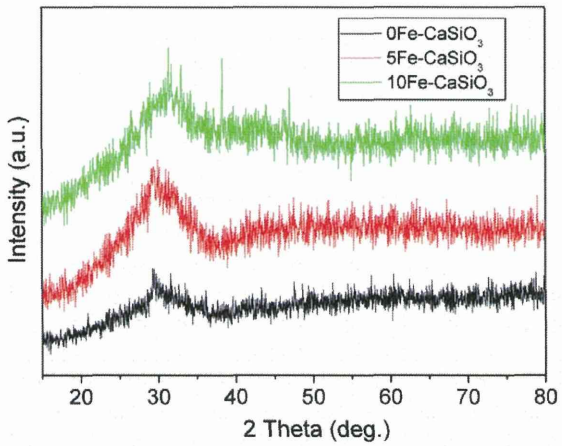

Figure 1. Wide-angle XRD patterns of mesoporous Fe-$CaSiO_3$ materials with different Fe substitution.

separated and dried at room temperature in vacuum for 48 h. The concentration of gentamicin in mesoporous Fe–$CaSiO_3$ materials was estimated by measuring the absorbance values at 256 nm before and after the loading [41]. Before determination, a calibration curve was recorded.

In vitro release of gentamicin from the drug-loaded mesoporous Fe–$CaSiO_3$ materials was carried out with a shaking bed at 37 °C. The drug-loaded mesoporous Fe–$CaSiO_3$ materials (0.5 g) were placed in a cover-sealed plastic bottle with 20 ml of the SBF solution, and the plastic bottle was fixed on a shaking bed with a shaking speed of 50 rpm. Gentamicin release was determined by UV analysis. The release medium was withdrawn at predetermined time intervals, and replaced with fresh SBF solution each time.

3. Results and discussion

3.1. Characterization of mesoporous Fe–CaSiO_3 materials

Figure 1 shows wide-angle XRD patterns of mesoporous Fe–$CaSiO_3$ materials. Similar to the previously reported mesoporous $CaSiO_3$, Sr–$CaSiO_3$ and magnesium–$CaSiO_3$ materials [7–9, 23, 24], mesoporous Fe–$CaSiO_3$ materials also lacked diffraction peaks related to the incorporated Fe ions except for a broad reflection at $2\theta = 25$–$35°$, which indicated the amorphous structure of Fe–$CaSiO_3$. Generally, amorphous $CaSiO_3$ has quicker apatite-formation ability due to the rapid release of Ca ions compared to α-$CaSiO_3$ and β-$CaSiO_3$ [42]. Therefore, the amorphous mesoporous Fe–$CaSiO_3$ materials could contribute to better bioactivity.

Figure 2 shows TEM images and EDS analysis of mesoporous Fe–$CaSiO_3$ materials. Well-ordered mesoporous structure can be clearly observed on mesoporous $CaSiO_3$ materials without Fe substitution (pore sizes about 5–6 nm). When 5 and 10% Fe were substituted for Ca in mesoporous $CaSiO_3$ materials, similarly ordered mesoporous channels with mesopore size of 5–6 nm could be seen, which suggested that the substitution of Fe for Ca did not change the mesoporous structure of mesoporous $CaSiO_3$ materials. From EDS analysis, Ca and Si were detected in the 0Fe–$CaSiO_3$ material, while the Fe, Ca and Si were clearly detected in the 5Fe–$CaSiO_3$ and 10Fe–$CaSiO_3$ materials, which indicated that Fe was successfully incorporated in the 5Fe–$CaSiO_3$ and 10Fe–$CaSiO_3$ materials. However, no iron oxide particles or aggregates could be detected, indicating that the Fe ions substituted the Ca ions in the framework of mesoporous $CaSiO_3$ materials, but did not form the magnetic nanoparticles inside the channels, which were similar to the previously reported results by Wu *et al* [39] and Gu *et al* [43].

Table 2. Structural parameters and gentamicin loading of mesoporous Fe–$CaSiO_3$ materials.

Samples	S_{BET} ($m^2\ g^{-1}$)	V_p ($cm^3\ g^{-1}$)	R_p (nm)	Drug loading capacity ($mg\ g^{-1}$)
0Fe–$CaSiO_3$	188.1	0.233	2.68	155
5Fe–$CaSiO_3$	137.2	0.208	2.87	125
10Fe–$CaSiO_3$	134.3	0.201	3.08	124

Elemental mapping was used to further confirm the distributions of Fe, Ca and Si in mesoporous Fe–$CaSiO_3$ materials. As shown in figure 3, the chemical compositions of Fe, Ca and Si were distributed homogeneously in the 5Fe–$CaSiO_3$ and 10Fe–$CaSiO_3$ materials, which were similar to the Zr-, Mg-, Sr- and Fe-substituted mesoporous bioactive glass prepared using sol–gel technique [16, 38]. Therefore, the results further indicated that Fe ions substituted Ca ions in the framework of mesoporous $CaSiO_3$ materials. In this study, mesoporous Fe–$CaSiO_3$ materials were prepared after the calcination at 600 °C for 6 h and reduction in 10%H_2 per 90%Ar atmosphere at 400 °C for 3 h, which might form magnetite in mesoporous Fe–$CaSiO_3$. Li *et al* [44] and Chen *et al* [45] have reported that hematite could transform to magnetite in the Fe-incorporated mesoporous bioactive glasses and mesoporous silica particles after the reduction treatment under hydrogen atmosphere.

N_2 adsorption–desorption isotherms of mesoporous Fe–$CaSiO_3$ materials are shown (figure 4) together with the corresponding pore size distributions. The data for the surface area, pore volume and peak pore size are listed in table 2. The Fe substitution in mesoporous $CaSiO_3$ did not change the mesoporous structure. The type IV isotherms with a type H1 hysteresis loop were similar to those of the reported mesoporous $CaSiO_3$ materials [7, 11, 23, 24], indicating the *P6mm* mesoporous structure of mesoporous Fe–$CaSiO_3$ materials. The BET surface areas (S_{BET}) of the 0Fe–$CaSiO_3$, 5Fe–$CaSiO_3$ and 10Fe–$CaSiO_3$ materials were 188.1 137.2 and 134.3 $m^2\ g^{-1}$, respectively. The single point adsorption total volume (V_P) at $P/P_0 = 0.97$ for the 0Fe–$CaSiO_3$, 5Fe–$CaSiO_3$ and 10Fe–$CaSiO_3$ materials were 0.233, 0.208 and 0.201 $cm^3\ g^{-1}$, respectively. The substitution of Fe for Ca in mesoporous $CaSiO_3$ decreased the surface area and pore volume, suggesting the decrease in the ordering degree of the 5Fe–$CaSiO_3$ and 10Fe–$CaSiO_3$ materials compared to the 0Fe–$CaSiO_3$ materials. The substitution of Fe for Ca in mesoporous Fe–$CaSiO_3$ might have generated defects in the mesoporous framework due to the difference of ion valence and radius, which has been reported in the substituted mesoporous bioactive glass [16]. Previous studies

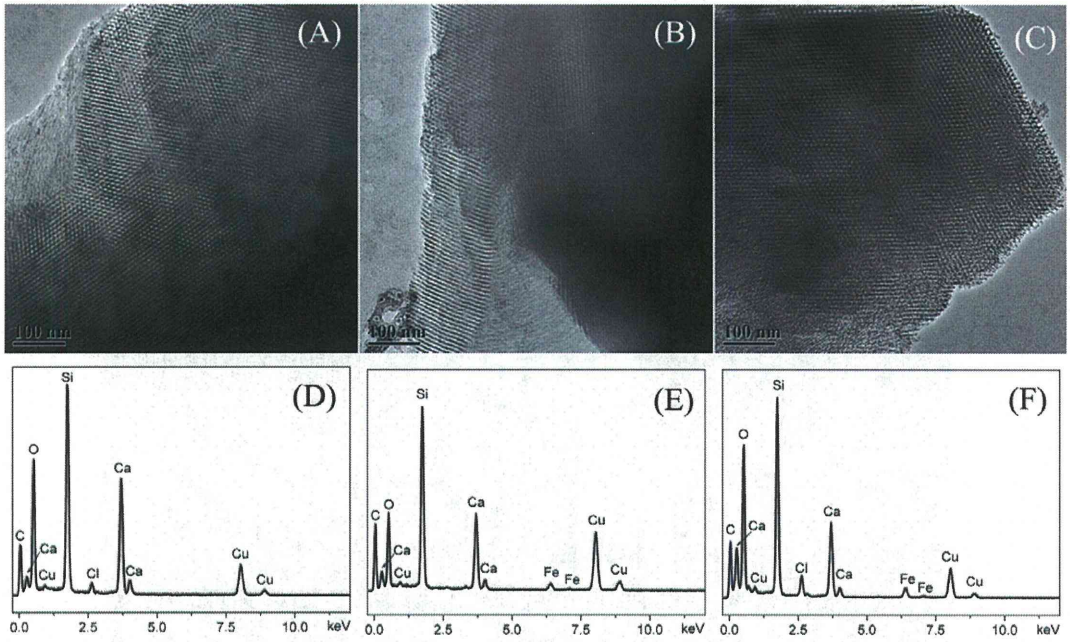

Figure 2. TEM images and the corresponding EDS analysis of mesoporous Fe-$CaSiO_3$ materials with different Fe substitution ((A) and (D): 0Fe-$CaSiO_3$; (B) and (E): 5Fe-$CaSiO_3$; (C) and (F): 10Fe-$CaSiO_3$).

have reported on the doping of Fe into glass-ceramics and Ca–P ceramics to make them magnetic, but they are unsuitable for drug delivery due to the absence of a nanoporous structure [30–33]. Furthermore, pore radius (R_P) distributions of mesoporous Fe–$CaSiO_3$ were narrow and peaked at 2.5–3 nm. In this study, the substitution of Fe for Ca in mesoporous $CaSiO_3$ materials decreased their surface area and pore volume. However, the mesoporous structure and large surface area of mesoporous Fe–$CaSiO_3$ materials ($>130\,m^2\,g^{-1}$) are beneficial for adsorption and sustained release of drugs.

3.2. Magnetic heating ability of mesoporous Fe–CaSiO$_3$ materials

The room temperature magnetization curves of the 0Fe–$CaSiO_3$, 5Fe–$CaSiO_3$ and 10Fe–$CaSiO_3$ materials are shown in figure 5(A). The magnetization of mesoporous Fe–$CaSiO_3$ materials increased with increase in Fe substitution. The 0Fe–$CaSiO_3$ materials have no magnetization due to their non-magnetic nature, whereas the 5Fe–$CaSiO_3$ and 10Fe–$CaSiO_3$ materials had a magnetization of 0.73 and 1.19 emu g^{-1} at 25 kOe, respectively, because the incorporated Fe ions formed a magnetite structure. Also, almost no hysteresis loops were observed on the curves of the 5Fe–$CaSiO_3$ and 10Fe–$CaSiO_3$ materials, suggesting superparamagnetic behavior. In practice, magnetic field generator that can operate under an AC frequency of 50 kHz–1.2 MHz and maximum magnetic field strength of 15 kA m^{-1} is considered safe for the human body [33]. In this study, the magnetic heating experiments were limited to an AC frequency of 200 kHz and magnetic field strength of 1.86 kA m^{-1}, respectively. Figure 5(B) shows the temperature increments of mesoporous Fe–$CaSiO_3$ materials in an alternating magnetic field. The 0Fe–$CaSiO_3$ suspension exhibited almost no increase in temperature during the experimental period. However, the temperatures of the 5Fe–$CaSiO_3$ and 10Fe–$CaSiO_3$ suspensions increased by 5.2 and 7.9 °C in 20 min, respectively. Therefore, the results indicated that the Fe substitution in mesoporous $CaSiO_3$ materials can produce magnetic property, and the magnetic strength of mesoporous $CaSiO_3$ materials can be tailored by changing the Fe substitution. Furthermore, magnetic mesoporous Fe–$CaSiO_3$ materials can generate heat to raise the temperature of the surrounding environment due to the delay in Neel relaxation of the magnetic moment in mesoporous Fe–$CaSiO_3$ materials [46], allowing for magnetic hyperthermia application.

3.3. Ion release and apatite formation ability of mesoporous Fe–CaSiO$_3$ materials

Studies demonstrated that the release of ions from biomaterials such as Si and Ca ions could stimulate the osteoblast proliferation and differentiation [47, 48]. On the other hand, the release of ions changes the pH around biomaterials, which will affect the cell growth and the osseointergration ability [18, 19]. Therefore, the release of Si, Ca and Fe ions from mesoporous Fe–$CaSiO_3$ in the SBF solution was investigated. As shown in figure 6, the release of Ca and Si ions increased with the increase in soaking time. However, the concentrations of Ca and Si ions decreased with increasing the Fe substitution, which might be because Fe ions provide more bonds to Si and O network than Ca ions, contributing to more stable network for mesoporous Fe–$CaSiO_3$ materials. The concentrations

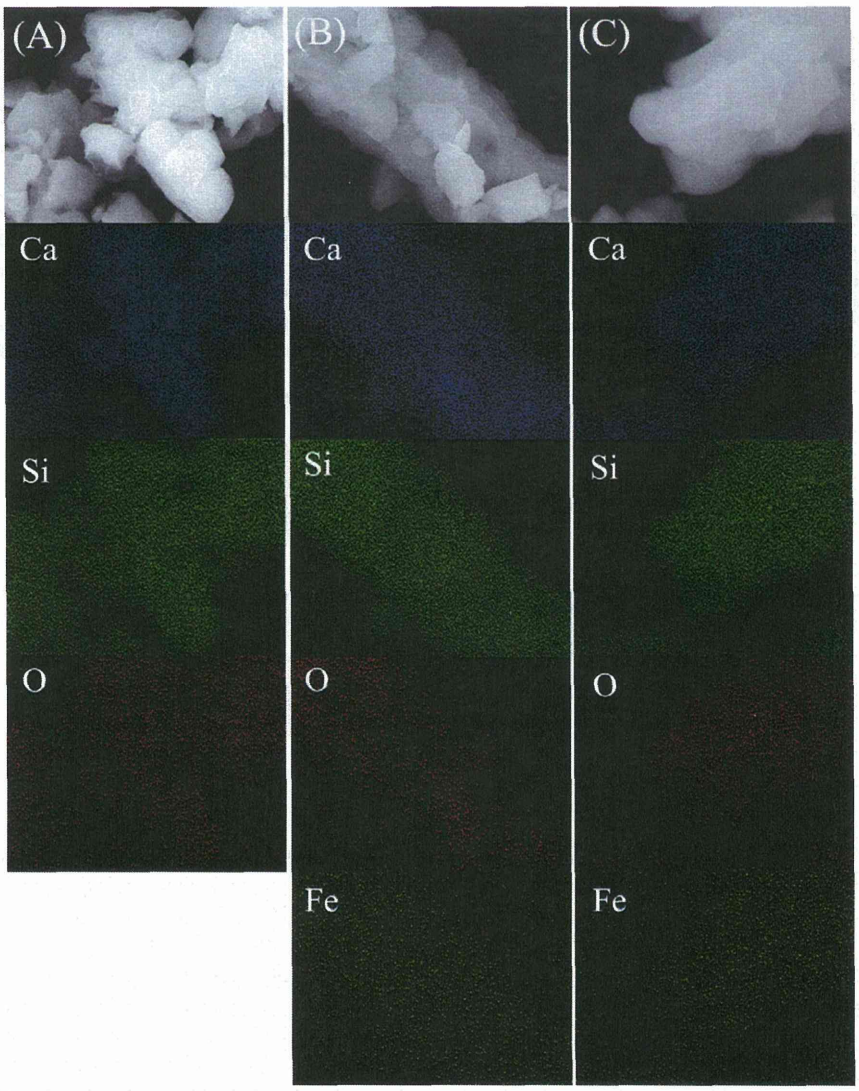

Figure 3. Element mappings of mesoporous Fe-$CaSiO_3$ materials with different Fe substitution ((A): 0Fe-$CaSiO_3$; (B): 5Fe-$CaSiO_3$; (C): 10Fe-$CaSiO_3$).

of Fe ions for the 5Fe–$CaSiO_3$ and 10Fe–$CaSiO_3$ materials were $<1\,mg\,ml^{-1}$ (not shown), which indicates that the concentration of released Fe ions was too low for ICP-OES detection. Another reason might be that the released Fe ions could be precipitated again due to the basic environment. The results were similar to those of the previously reported Fe-incorporating mesoporous bioactive glass [38, 39]. Figure 6(C) shows the pH changes of the SBF solutions after soaking mesoporous Fe–$CaSiO_3$ materials. It can be observed that the pH values of mesoporous Fe–$CaSiO_3$-soaked SBF solutions decreased with increase in the Fe substitution in mesoporous Fe–$CaSiO_3$ materials, and that the pH values could be stabilized at 8.2, 7.9 and 7.7 after 7 days of soaking for the 0Fe–$CaSiO_3$, 5Fe–$CaSiO_3$ and 10Fe–$CaSiO_3$ materials, respectively. It indicated that the substitution of Fe for Ca in mesoporous $CaSiO_3$ materials improved the ability to stabilize the pH environment, which is beneficial for cell growth on mesoporous Fe–$CaSiO_3$ materials.

It has been accepted that the apatite-formation ability of a biomaterial in SBF solution is useful for predicting the *in vivo* bone bioactivity of a biomaterial, and the formation of apatite layer shows the ability of a biomaterial to form interfacial bonds with tissues when in contact with physiological fluid [49]. In this study, the apatite formation on mesoporous Fe–$CaSiO_3$ materials after soaking in the SBF solution was investigated by SEM with EDS analysis. As shown in figure 7, after soaking mesoporous Fe–$CaSiO_3$ materials in SBF for 3 days, a new layer of apatite particles that had a diameter of several micrometers and flower morphology were formed on the surface of the pellets. Phosphorus signals appeared in the EDS spectra of mesoporous Fe–$CaSiO_3$ materials after soaking in the SBF, and the Ca/P ratio was 1.79, 1.92 and 1.95 for the 0Fe–$CaSiO_3$, 5Fe–$CaSiO_3$ and 10Fe–$CaSiO_3$ materials, respectively. The results indicated that mesoporous Fe–$CaSiO_3$ materials possess good apatite-formation ability in physiological fluid. On the other hand, it can also be

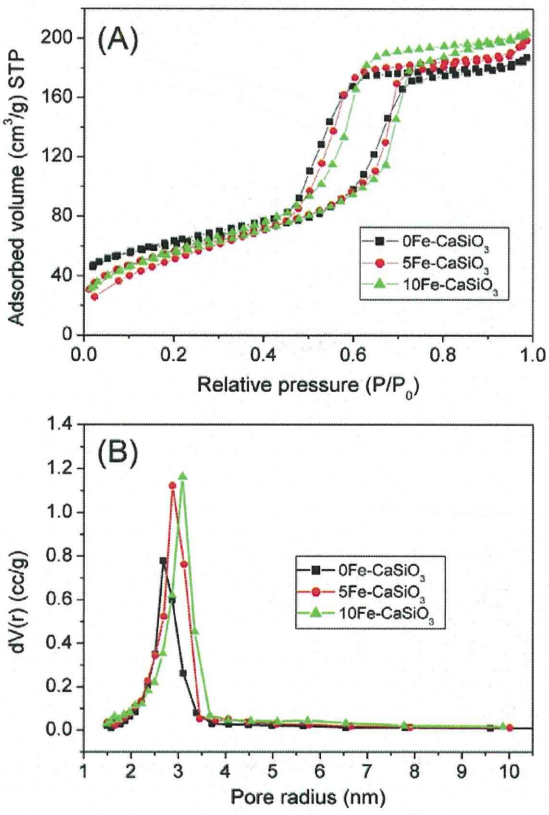

Figure 4. N_2 adsorption-desorption isotherms (A) and the corresponding pore size distributions (B) of mesoporous Fe-$CaSiO_3$ materials.

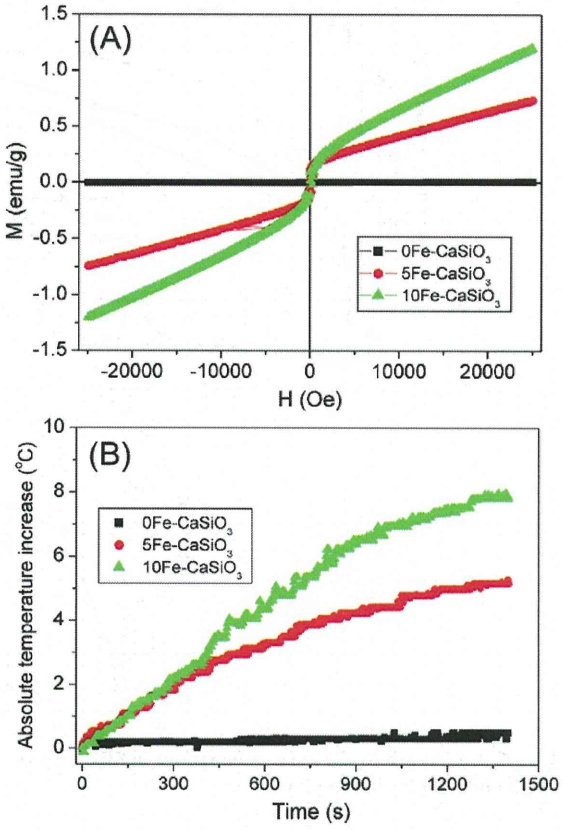

Figure 5. (A) Magnetization curves as a function of the applied magnetic field for different mesoporous Fe-$CaSiO_3$ materials at room temperature; (B) magnetic heating curves of different mesoporous Fe-$CaSiO_3$ materials in an alternating magnetic field.

observed that the apatite layer exhibited a small decrease in thickness for mesoporous Fe–$CaSiO_3$ materials with increasing Fe substitution, suggesting a small decrease in the apatite-formation rate. Generally, the release of Ca ions from a biomaterial accelerates the apatite formation due to the increase of Ca concentration in the SBF solution. In this study, the Ca ions were released from the 0Fe–$CaSiO_3$, 5Fe–$CaSiO_3$ and 10Fe–$CaSiO_3$ materials, but the Ca ions release rates showed small decrease with increase in the Fe substitution in mesoporous $CaSiO_3$ materials, which contributed to small decrease in the apatite-formation rate for mesoporous Fe–$CaSiO_3$ materials with increase in the Fe substitution.

3.4. Cytotoxicity evaluation of mesoporous Fe–CaSiO$_3$ materials

To evaluate the cytotoxicity of mesoporous Fe–$CaSiO_3$ materials, the elution cell culture assay (also known as extract dilution) was used in this study. The cytotoxic effect of mesoporous Fe–$CaSiO_3$ extracts on osteoblast-like MC3T3-E1 cells is shown in figure 8. It can be seen that there were no cytotoxic effects on MC3T3-E1 cells for mesoporous Fe–$CaSiO_3$ materials from a low extract concentration (6.25 mg ml^{-1}) to a high extract concentration (50 mg ml^{-1}) after 7 days. The 5Fe–$CaSiO_3$ and 10Fe–$CaSiO_3$ extracts had comparable cell viability compared to the 0Fe–$CaSiO_3$ extracts. However, the extracts of mesoporous Fe–$CaSiO_3$ materials with concentrations from 6.25 to 25 mg ml^{-1} improved the proliferation of MC3T3-E1 cells compared to the blank control. The corresponding ion concentrations of mesoporous Fe–$CaSiO_3$ extracts for cell culture are listed in table 3. The Ca, Si and Fe ions were released from mesoporous Fe–$CaSiO_3$ materials in culture medium. The Ca and Si ion concentrations respectively ranged from 72.7 to 96.3 mg ml^{-1} and 4.9 to 63.1 mg ml^{-1}, while the Fe ion concentrations were lower than 2.8 mg ml^{-1}. Previous studies showed that high concentrations of Ca, Si and Fe ions can result in excessive cytotoxicity [25, 50]. In this study, the results indicated that the 0Fe–$CaSiO_3$, 5Fe–$CaSiO_3$ and 10Fe–$CaSiO_3$ extracts were not cytotoxic to MC3T3-E1 cells and could induce osteoblast activity, suggesting that the released Ca, Si and Fe ions from mesoporous Fe–$CaSiO_3$ materials are in the feasible levels and are very useful for bone regeneration.

3.5. Gentamicin release from mesoporous Fe–CaSiO$_3$ materials

Besides the magnetic heating ability and bioactivity, mesoporous Fe–$CaSiO_3$ materials can also efficiently load